Koc. J. Sci. Eng., 6(2): (2023) 172-180 https://doi.org/10.34088/kojose.1252944

Kocaeli University

Kocaeli Journal of Science and Engineering

http://dergipark.org.tr/kojose

First-Principles Study of Titanium and Lithium Adsorption on Perfect and Defective Hexagonal Boron Nitride Monolayer Under Effects of Charging

Bahadır SALMANKURT [1, *]

[1] *Distance Education Center, Sakarya University of Applied Sciences, Sakarya, 54050, Turkey,* ***ORCID:*** *0000-0001-7611-9647*

Article Info

Research paper

Received *: February 18, 2023*
Accepted *: April 25, 2023*

Keywords

Monolayer
Density Functional Theory
Charging
Electronic properties
Semiconductor

Abstract

Single Titanium (Ti) and Lithium (Li) atoms adsorption on Pristine and defective hexagonal boron nitride (P-h-BN and BV-h-BN) monolayer were employed using Density Functional Theory (DFT) under effect of charging. Obtained data reveal that Li adsorption on P-h-BN is weak, while Ti adsorption on P-h-BN is strong. When Ti and Li atoms interact with P-h-BN surface, Ti and Li generate 4 μB/cell and 1 μB/cell magnetic moments, respectively. The extraction of an electron from the systems leads to a considerable rise in the adsorption energy, notably in the case of Li-P-h-BN. There is a notable decrease in the band gap of Ti-P-h-BN in both the charged states, especially in the electron-added state. Removing an electron from the Li-P-h-BN system results in a non-magnetic state and a significant increase of the band gap to 4.07 eV. Ti-BV-h-BN system shows significantly stronger adsorption energy due to the d-orbitals of the Ti atom. When an electron is added to the systems, the interaction energy between Ti and BV-h-BN decreases, while the interaction energy between Li and BV-h-BN increases. Moreover, removing an electron from Ti-BN-h-BN increases the band gap to 2.29 eV and the disappearance of the magnetic moment.

1. Introduction

Semiconductors have been regarded as a cornerstone for numerous electronic applications, such as electromedical devices, personal computers, wireless communications, automobiles, and so on. As a result, demand for the most popular semiconductor, silicon, has consistently seen robust growth in recent years [1]. The COVID-19 pandemic has further fueled this momentum, particularly in the automotive and lubricant industries [2]. Hence, the discovery of effective materials for technological applications other than silicon-based electronics is becoming increasingly urgent.

Two-dimensional (2D) materials can support the demand from the silicon-based electronic world. The discovery of Graphene (GR) in 2004 has tremendously aroused interest in the electronic [3]. After this discovery, scientists have been searching for stable and convenient materials in many application areas for years, and they have found materials such as phosphorene, hexagonal boron nitride (h-BN), silicene, stanene, transition metal di-chalcogenides (TMDCs), etc. [4-7]. Although GR has unique properties, its non-band gap state is an obstacle for most electronic compounds [7]. So, stable and wide band gap 2D material seems to be required from a wide range of industries [7-8].

h-BN monolayer may be exactly what scientists and engineers are looking for in the mentioned fields. Because its band gap theoretically and experimentally was found to be 4.55 and 6.1 eV, respectively [8-9]. Moreover, h-BN is as stable as GR [8]. According to the obtained knowledge, it seems very reasonable to consider h-BN monolayer as potential material for future studies [8-12].

Examining the history of h-BN can provide valuable insight into the material's significance for technological applications. The formation of a highly regular self-assembled BN nanostructure with a periodicity of 3.22 nm on Rh (111) by CVD of borazine ("NanoMesh") was first obtained by *Corso et al*., and the BN monolayer structure was modeled by *Laskowski et al.* [8-9]. From then until now, many studies related to h-BN monolayer have been performed [10-21].

* Corresponding Author: bsalmankurt@gmail.com

In recent years, functionalization, or doped h-BN with Lithium (Li), has been explored to enhance its properties and broaden its potential applications [11-12]. Li functionalized or doped h-BN has been shown to exhibit improved electrical conductivity, thermal stability, and catalytic activity compared to pristine h-BN [12,15]. This has made Li functionalized or doped h-BN a promising material for various energy-related applications, such as batteries and supercapacitors [12,15].

Moreover, doping or functionalizing h-BN with transition metals, such as Iron (Fe), Nickel (Ni), and Titanium (Ti), has been shown to introduce localized states into the bandgap and modify its electrical, magnetic, and optical properties [16-21]. Furthermore, the adsorption of Ti at a vacancy site in an h-BN sheet is effortless [16]. Moreover, the incorporation of Ti into h-BN materials leads to the formation of narrow-band semiconductors, which is promising for novel technological devices [18]. This makes h-BN doped or functionalized with transition metals of great interest for the development of new spintronic devices, sensors, and catalysts. Compared to electronic devices, faster reading and writing of data in storage can be achieved through spintronics, which has the potential to replace silicon-based semiconductor devices [22]. Thus, we have also focused on Ti modified h-BN in this work.

Furthermore, modifying the net charge of the systems leads to a significant impact on the binding mechanism. In this way, the charging highly affects the band structures, distance between atoms, and adsorption energies. [23]. A better understanding of these effects can provide valuable insights into the behavior and interactions of charged 2D atoms and can play an important role in advancing our understanding of these systems.

2. Methods

The calculations were performed using the Siesta code, which uses a linear combination of pseudoatomic orbitals (LCAO) as basis functions and implements Density Functional Theory (DFT) [24-26]. The Perdew-Burke-Ernzerhof (PBE) functional within the generalized gradient approximation (GGA) was used as the exchange-correlation potential [27]. The Grimme method was employed to calculate the energetics and interactions of the monolayer and atom systems, which is a correction for Van der Waals (vdW) interactions [28]. A typical vdW effect in the literature is around 3 Å and becomes important for interactions at this distance. However, as the interaction distance decreases, the vdW effect becomes relatively less significant.

The sample was modeled using a 2D periodic 5x5 supercell with a vacuum layer of 20 Å to avoid interactions between periodic images. A plane wave cutoff energy of 250 Ry was used, and the Brillouin zone (BZ) was sampled using a Monkhorst-Pack grid of 5x5x1 k-points [29]. The geometry optimization was performed using the conjugate gradient (CG) method until the forces on each atom were less than 0.01 eV/Å.

To investigate the electronic properties of the systems, the band structures were calculated. The band structures were calculated along high-symmetry lines in the BZ. The Fermi level was determined by integrating the Density of States (DOS) up to the number of electrons in the system. The adsorption energy (E_{ads}) of a single Li or Ti atom on Pristine h-BN (P-h-BN) or Boron-Vacancy h-BN (BV-h-BN) monolayer is given by the formula:

$$E_{ads} = E_{sys} - E_{BN} - E_X \quad (1)$$

where E_{sys} is the total energy of P-h-BN or BV-h-BN monolayer with adsorbed single Li or Ti atoms, E_{BN} is the total energy of the P-h-BN or BV-h-BN monolayers, and E_X indicates the energy for isolated single Li or Ti atoms in a vacuum. On the other hand, when the net total charge of the systems changes, the above-mentioned formula is no longer suitable. This is because a change in the net charge of the systems fundamentally affects the binding mechanism. Instead of using the formula, it is a better choice to use the pulling method. In this method, one should gradually pull the atoms out from the layers along a perpendicular direction to the h-BN surface until the interaction energy between the atoms and the layer disappears [23,30]. To carry out this process, it is important to first fix the corner atoms of the monolayer to prevent movement during the pulling process. Also, some parameters should be changed in the Siesta Code. The *tot_charge* tag is used to determine the total charge of the system in the Siesta Code. Its default value is zero, indicating a neutral state. +1 represents the removal of an electron from the corresponding unit cell, while -1 represents the addition of an electron to the cell. After the parameter was modified, the relaxation calculation was performed again. For example, when one electron was added to a 5x5 h-BN cell using *tot_charge=-1* tag, the charge was uniformly distributed on the h-BN surface, leading to an extra 0.12 Coulomb per square meters (-0.12 C/m^2) on h-BN surface.

The total energy difference between the relaxed state and the final step in the pulled state gives the pulling energy value, which can be defined as follows:

$$E_P = E_T[Relaxed] - E_T[Pulled\_final] \quad (2)$$

where E_P represents the energy required for the adsorption of charged systems. $E_T[Relaxed]$ represents the total

energy of the system that is in the relaxed state, while $E_T[Pulled\_final]$ represents the total energy of the system that is the final step in the pulled state. E_P gives us the same results with E_{ads}.

To draw geometric structures, Vesta software was used [31].

3. Results and Discussion

3.1. The Structural and Electronic Properties of P-h-BN and BV-h-BN

First of all, the lattice constants of 1x1 P-h-BN (a, b) were calculated, and the obtained data reveal that the values of a, b for 1x1 P-h-BN have been found to be 2.51 Å. This value is in good agreement with previous studies [10-20]. Additionally, the bond distance between the N and B atoms was calculated to be 1.45 Å, within the previous data range [10-20].

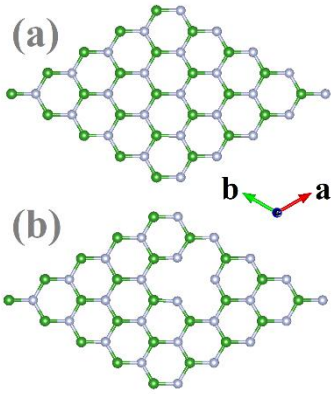

Figure 1. Schematic illustration of a top view of a) P-h-BN and b) BV-h-BN. The green ball stands for the B atom, and the gray one is for the N atom.

Next, the size of 1x1 P-h-BN expanded to 5x5, as shown in Figure 1(a), to investigate electronic and other properties. The first of these is to calculate band structures.

The band gap of P-h-BN has been calculated as 4.55 eV, as seen in Figure 2(a), and is very close to the data in the literature [10-20].

Finding a perfect crystal in nature is quite difficult, and defects always occur. One of the possible defects is caused by atomic vacancy. So, the effect of vacancy defects has been considered.

Due to the more favorable B vacancy on h-BN monolayer (BV-h-BN) compared to regular N vacancy, B vacancies on monolayers have been extensively studied [13,15,32]. The removal of a B atom from the layer does not result in a significant change in the structure after structural relaxation (as seen in Figure 1(b)); however, magnetic moment arises due to the presence of non-bonding atoms. Because of this, a spin-polarized state has been considered. In this case, there will be three N atoms that cause a missing bond, which leads to 3 μB/cell of magnetic moment, in line with previous study [32]. Naturally, this situation also caused changes in the band structure. The band structures of BV-h-BN are depicted in Figure 2(b). Obtained data reveal that there is no band gap for the spin-down (Blue lines in Figure 2(b)) state. However, spin-up has a band gap of 4.65, which is almost the same as a pristine state. This implies that BV-h-BN is in a semimetallic state, as previously reported in studies. [15,32].

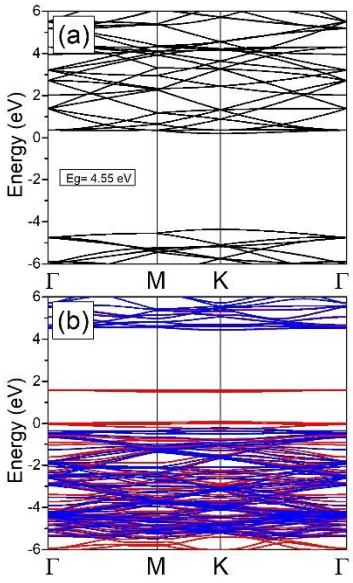

Figure 2. Electronic band structures of a) P-h-BN and b) BV-h-BN. The Fermi level is set to zero. Black lines mean a non-magnetic state. Red lines indicate a spin-down state, while blue lines are a spin up state. Eg indicates band gap value in eV.

The results obtained in this section demonstrate the reliability of the study and can be easily considered in the following sections.

3.2. Binding Mechanism of Li or Ti Functionalized P-h-BN

In this section, the focus is on Li/Ti functionalized P-h-BN (Li/Ti-P-h-BN). The calculation that included spin-polarization was also considered because bare Ti and Li atoms are spin-polarized.

The calculation started with atom-monolayer interaction. The atom was placed at a location that is 3 Å away from the surface of P-h-BN, then the system was relaxed. This was applied to both Ti and Li atoms. As we can see from Figure 3, both atoms preferred the hollow site of P-h-BN. Furthermore, the E_{ads} was calculated using the formula provided in the Methods section, and the results are presented in Table 1. Obtained data reveal that the E_{ads} of

Li-P-h-BN is relatively weaker than that of Ti-P-h-BN.

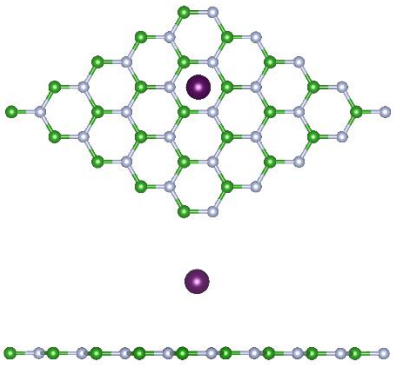

Figure 3. Schematic illustration of top and side view of Li/Ti-P-h-BN. The green ball stands for B atom and the gray one is for N atom. The purple indicates Li or Ti atoms.

This is probably due to the role of d-electrons, which play an important role in the E_{ads} [10]. So, interacting P-h-BN with d-electron atoms can cause stronger E_{ads}, which might be considered in a situation where atoms need to be strongly held on the surface. As we know, typically, an inverse relationship exists between energy and atomic distances, whereby an increase in interaction between the atom and layer results in a corresponding decrease in atomic distances. The minimum distances between the atom and the monolayer were considered to deeply understand interaction mechanism for all calculations. For example, the minimum atomic distances between Ti and Li atoms with P-h-BN were calculated as 2.25 Å and 3.62 Å, respectively. The results have been calculated as expected.

Table 1. The E_{ads} of Li/Ti-P-h-BN (in eV). N1, Neutral and P1 indicate Q=-1e/cell, Q=0 and Q=+1e/cell case of GGA-vdW.

Cases	Li	Ti
ΣQ=-1 (N1)	-0.06	-1.61
Neutral	-0.19	-0.72
GGA-vdW [11]	-0.02	-
GGA-vdW [10]	-	-1.27
GGA-vdW [12]	-0.16	-
ΣQ=+1 (P1)	-1.55	-2.03

Next, the magnetic moments of the systems have been considered. As can be seen from Table 2, it was found that Ti-P-h-BN has a magnetic moment of 4 μB/cell, while that of the Li-P-h-BN atom is 1 μB/cell. The result for Ti-P-h-BN is consistent with previous studies [10]. On the other hand, the effects of changing the net charge in the supercell were examined. It is known that the net charge of the system can be manipulated by adding or removing an electron to or from the system [23]. This has a significant impact on the E_P and electronic properties [23,30]. Here, N1 refers to adding one electron to the supercell, while P1 represents removing one electron from the supercell.

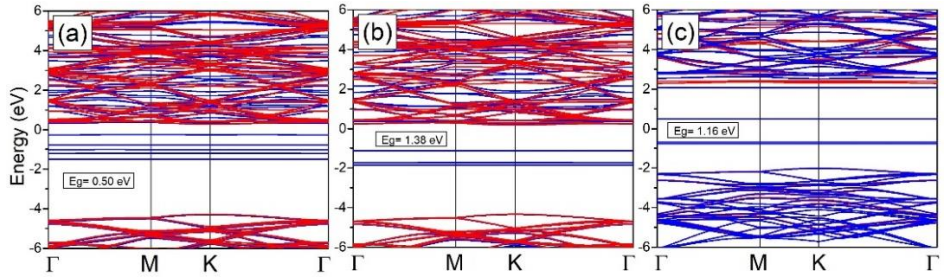

Figure 4. The band structures of (a) Q=-1e/cell, (b) Neutral and (c) Q=+1e/cell case for Ti-P-h-BN. The Fermi level is set to zero. Red lines indicate a spin-down state, while blue lines are a spin-up state. Eg indicates band gap value in eV.

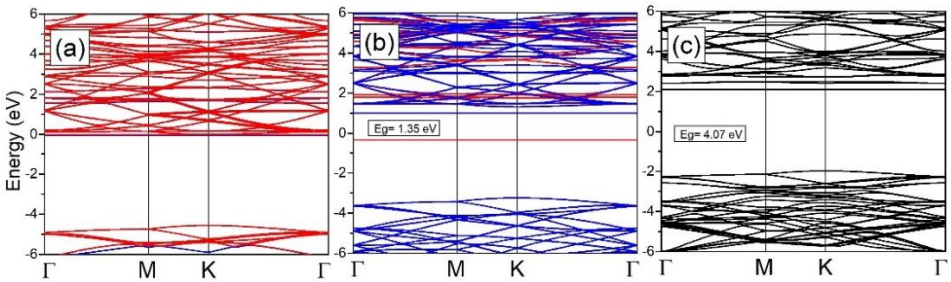

Figure 5. The band structures of (a) Q=-1e/cell, (b) Neutral, and (c) Q=+1e/cell case for Li-P-h-BN. The Fermi level is set to zero. Black lines mean a non-magnetic state. Red lines indicate a spin-down state, while blue lines are a spin-up state. Eg indicates band gap value in eV.

Table 2. The magnetic moment of Li/Ti-P-h-BN (in μB/cell). N1, Neutral, and P1 indicate Q=-1e/cell, Q=0, and Q=+1e/cell case of GGA-vdW.

Cases	Li	Ti
ΣQ=-1 (N1)	0.03	5.00
Neutral	1.00	4.00
GGA-vdW [10]		4.00
ΣQ=+1 (P1)	0.00	3.00

As can be seen from Table 1, removing an electron from the system results in a significant increase in the E_P, especially for Li-P-h-BN. However, when one electron is added to the system, the E_P of Li-P-h-BN becomes very low, compared to P1 state. Therefore, Li atoms can be kept on the P-h-BN layer by removing electrons and released easily by adding electrons. This method may be used in Li-ion based materials.

On the contrary, the change in net charge (N1 or P1) leads to an increase in E_P for the Ti-P-h-BN system. Charging the system also affects the electronic properties. For instance, the band gap of Ti-P-h-BN decreases in both the N1 and P1 states, especially in the N1 state (as seen in Figure 4). Thus, it is possible to manipulate band gap. In the case of Li-P-h-BN, significant events occur. When an electron is removed from the system, a non-magnetic state is created and the band gap significantly increases to 4.07 eV. When an electron is added, a very small magnetic moment is observed and no band gap is observed (Figure 5). Hence, changing the net charge of the system provides the opportunity to use the material in many electronic devices. Furthermore, the calculated magnetic moments are given in Table 2. Obtained daha reveal that magnetic moments of the systems are highly affected by the changing the net charge.

3.3. Binding Mechanism of Li or Ti (Li/Ti) doped BV-h-BN

The most stable configuration of Li/Ti-BV-h-BN is shown in Figure 6. For Ti-BV-h-BN, the minimum distance between Ti-N atoms is found to be 1.87 Å, while for Li-BV-h-BN, the minimum distance of Li-N atoms is 2.00 Å.

Here, the vacancy site of the monolayer has interacted with Ti or Li atoms and then the E_{ads} was calculated. As seen in Table 3, the strong E_{ads} is noticed, which is in good agreement with previous studies [15-21]. However, E_{ads} in Ti-BV-h-BN system is much stronger than in Li-BV-h-BN. Because transition metals with d-orbitals interact more strongly with surfaces [16-21].

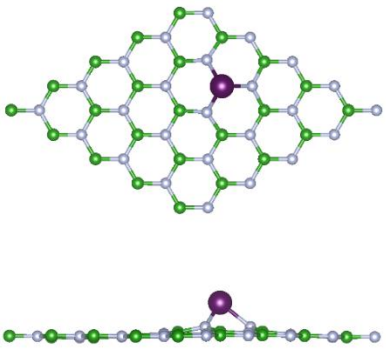

Figure 6. Schematic illustration of top and side view of Li/Ti-BV-h-BN. The green ball stands for B atom and the gray one is for N atom. The purple indicates Li or Ti atoms.

When an electron was added to the systems, the interaction between Ti and BV-h-BN decreased, while the interaction between Li and BV-h-BN increased, vice versa. This is due to the different charge distributions between Ti/Li and BV-h-BN, which can be understood by analyzing the molecular orbitals with magnetism.

Table 3. The E_P of Li/Ti-BV-h-BN (in eV). N1, Neutral and P1 indicate Q=-1e/cell, Q=0 and Q=+1e/cell case of GGA-vdW.

Cases	Li	Ti
ΣQ=-1 (N1)	-5.09	-9.32
Neutral	-4.61	-11.82
GGA-vdW [15]	-5.30	
GGA [16]		-11.39
GGA-vdW [17]		-11.59
GGA-vdW [18]		-11.60
GGA-vdW [19]		-11.48
GGA-vdW [20]		-12.70
GGA-vdW [21]		-12.90
ΣQ=+1 (P1)	-3.01	-13.12

Herein, *Wang. et al.* have used molecular orbital theory (MOT) to show the mechanism of the magnetic properties of Ti-BV-h-BN [22]. In the mentioned study, the magnetic moment of Ti-BV-h-BN was found to be 1 μB/cell because a spin electron was left in the orbital $\pi_{E'}$. Also, there were found to be five orbitals that did not have any electrons.

When we added an electron to the same system, one of the orbitals that did not have an electron was filled. This resulted in two half-filled orbitals, corresponding to a magnetic moment of 2 μB/cell. However, when an electron is removed from the same system, the electron occupying the orbital $\pi_{E'}$ is removed, resulting in a non-magnetic state.

But the same story is not seen for Li-BV-h-BN, where the magnetic moment increased by adding an electron and

decreased by removing an electron. So, changing the net charge gives rise to different results in the magnetic moment for both systems, resulting in different charge distributions.

Afterwards, the band structures of the systems were calculated and described in Figures 7 and Figures 8. For both neutral systems, the band gap was observed. However, the band structures became different by manipulating the net charge. For example, if an electron was removed from Ti-BV-h-BN, the band gap increased to 2.29 eV, and the magnetic moment disappeared. On the other hand, for Li-BV-h-BN, it is possible to eliminate the band gap by changing the net charge of the system.

Table 4. The magnetic moment of Li/Ti-BV-h-BN (in μB/cell). N1, Neutral, and P1 indicate Q=-1e/cell, Q=0, and Q=+1e/cell case of GGA-vdW.

Cases	Li	Ti
ΣQ=-1 (N1)	1.00	2.00
Neutral	2.00	1.00
GGA [13]	-	1.00
GGA [14]	-	1.00
ΣQ=+1 (P1)	3.00	0.00

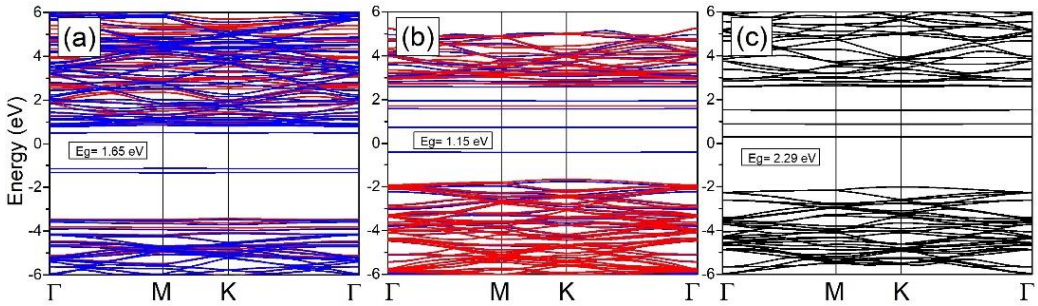

Figure 7. The band structures of (a) Q=-1e/cell, (b) Neutral, and (c) Q=+1e/cell case for Ti-doped h-BN. The Fermi level is set to zero. Black lines mean a non-magnetic state. Red lines indicate a spin-down state, while blue lines are a spin-up state. Eg indicates band gap value in eV.

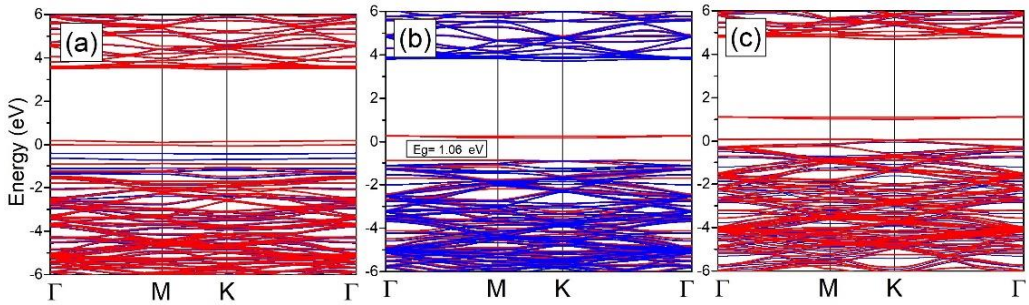

Figure 8. The band structures of (a) Q=-1e/cell, (b) Neutral, and (c) Q=+1e/cell case for Li-doped h-BN. The Fermi level is set to zero. Red lines indicate a spin-down state, while blue lines are spin-upup state. Eg indicates band gap value in eV.

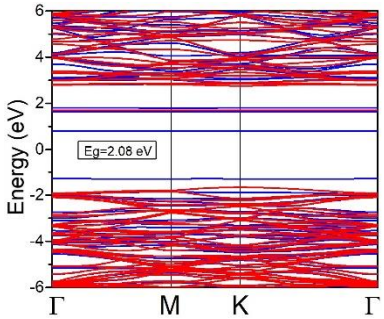

Figure 9. The band structure of Ti-BV-h-BN with DFT+U. The Fermi level is set to zero. Red lines indicate spin down state, while blue lines are spin up state. Eg indicates band gap value in eV.

Further, the effects of the E_{ads} and band structure have been demonstrated using the DFT+U method [33-35], with Ti-BV-h-BN serving as an example. For Ti, U value of 3.3 eV, as indicated in the literature [22], was chosen. The E_{ads} was found to be -7.93 eV, weaker than the GGA results. The impact of the DFT+U method on the band structure was also analyzed. As known, GGA generally underestimates the band gap [33-35]. With the implementation of the DFT+U method, the band structure of Ti-BV-h-BN changed, resulting in an increase in the band gap from 1.15 eV to 2.08 eV, as illustrated in Figure 9. The obtained data is in good agreement with previous findings [22].

The study has been extended to investigate the effect of the N-vacancy defect (NV-h-BN) with Ti/Li atom (Ti/Li-NV-h-BN). N-vacancy in the h-BN monolayer can be

observed, making the investigation of the N-vacancy defect an important matter. Initially, an N atom was removed, and then the system was relaxed. The results indicate that removing an N atom induced 1 μB/cell of magnetic moment. Subsequently, Ti/Li atoms interacted with the vicinity of the N-vacancy site, and after full relaxation, the band structures were obtained and presented in Figure 10. Specifically, Figure 10(a) indicates a band gap of 0.98 eV with up spin to down spin transition, which is different from Figure 7(b). On the other hand, there is no band gap for Li-NV-h-BN, as illustrated in Figure 10(b). These changes are not limited to the band structures only. The E_{ads} values were found to be -4.20 eV and -2.23 eV for the Ti-NV-h-BN and Li-NV-h-BN cases, respectively, while the total magnetic moments were calculated as 5 μB/cell for Ti-NV-h-BN and 2 μB/cell for Li-NV-h-BN.

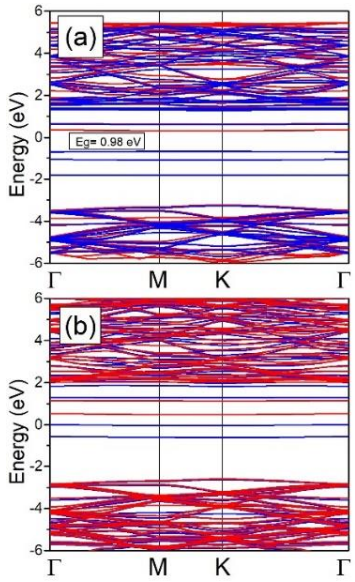

Figure 10. The band structures of (a) Ti-NV-h-BN, (b) Li-NV-h-BN. The Fermi level is set to zero. Red lines indicate a spin-down state, while blue lines are a spin up state. Eg indicates band gap value in eV.

4. Conclusions

The data obtained from the study showed that the adsorption energy of Ti-P-h-BN is stronger than that of Li-P-h-BN, and the Ti-P-h-BN system has a magnetic moment of 4 μB/cell, while that of Li-P-h-BN is 1 μB/cell. The net charge of the system can be manipulated by adding or removing an electron, which results in a significant increase in the interaction, especially for Li-P-h-BN. In the case of Ti-P-h-BN, the band gap decreases in both the N1 and P1 states, particularly in the N1 state. Meanwhile, removing an electron from Li-P-h-BN leads to a non-magnetic state and a significant increase in the band gap to 4.07 eV. The magnetic moments of the systems are highly affected by changing the net charge. On the other hand, the adsorption energy in the Ti-BV-h-BN system is much stronger than that in the Li-BV-h-BN system, which can be attributed to the strong interaction of transition metals with d-orbitals with surfaces. Adding an electron to the systems decreased the interaction between Ti and BV-h-BN, while it increased the interaction between Li and BV-h-BN. Finally, removing an electron from the Ti-BN-h-BN system increased the band gap to 2.29 eV, and the magnetic moment disappeared. As a result, it is clear that the modified h-BN will be of great benefit to the needs of the silicon-based semiconductor world, and experimental applications of such studies should be developed more.

Declaration of Ethical Standards

The author of this article declares that the materials and methods used in this study do not require ethical committee permission and/or legal-special permission.

Conflict of Interest

The author declare that they have no known competing financial interests or personal relationships that could have appeared to influence the work reported in this paper.

Acknowledgements

The numerical calculations reported in this paper were fully performed at TUBITAK ULAKBIM, High Performance and Grid Computing Center (TRUBA resources).

References

[1] Knobloch T., Illarionov Y. Y., Ducry F., Schleich C., Wachter S., Watanabe K., Grasser T., 2021. The performance limits of hexagonal boron nitride as an insulator for scaled CMOS devices based on two-dimensional materials. Nature Electronics, **4**(2), pp. 98-108.

[2] Gupta S., 2022. Chip demand pushes automotive and lubricant industry changes. Tribology & Lubrication Technology, **78**(3), pp. 22-24.

[3] Geim A. K., Novoselov K. S., 2007. The rise of graphene. Nature materials, **6**(3), pp. 183-191.

[4] Gürel H. H., Salmankurt B., 2021. Quantum Simulation of the Silicene and Germanene for Sensing and Sequencing of DNA/RNA Nucleobases. Biosensors, **11**(3), pp. 59-62.

[5] Salmankurt B., Gürel, H. H., 2022. Two-Dimensional Nanomaterials Based Biosensors. In Progress in Nanoscale and Low-Dimensional Materials and Devices: Properties, Synthesis, Characterization, Modelling and Applications. 1st ed., Springer, Berlin, Germany, pp. 767-778.

[6] Elias C., Valvin P., Pelini T., Summerfield A., Mellor C. J., Cheng T. S., Cassabois, G., 2019. Direct bandgap crossover in epitaxial monolayer boron nitride. Nature Communications, **10**(1), pp. 2639-2646.

[7] Wang B., Sun Y., Ding H., Zhao X., Zhang L., Bai J., Liu K., 2020. Bioelectronics-related 2D materials beyond graphene: fundamentals, properties, and applications. Advanced Functional Materials, **30**(46), pp. 2003732-2003761.

[8] Corso M., Auwarter W., Muntwiler M., Tamai A., Greber T., Osterwalder J., 2004. Boron nitride nanomesh. Science, **303**(5655), pp. 217-220.

[9] Laskowski R., Blaha P., Gallauner T., Schwarz K., 2007. Single-layer model of the hexagonal boron nitride nanomesh on the Rh (111) surface. Physical Review Letters, **98**(10), pp. 106802-106806.

[10] Li S., Zhou M., Li M., Lu G., Wang X., Zheng F., Zhang P., (2018). Adsorption of 3d, 4d, and 5d transition-metal atoms on single-layer boron nitride. Journal of Applied Physics, **123**(9), pp. 095110-095116.

[11] Hwang Y., Chung Y. C., 2013. Lithium adsorption on hexagonal boron nitride nanosheet using dispersion-corrected density functional theory calculations. Japanese Journal of Applied Physics, **52**(6S), pp. 06GG08-06GG12.

[12] Sarikurt S., 2019. A first-principles investigation of Lithium Adsorption and Diffusion on BN, AlN and GaN monolayers. Eskişehir Technical University Journal of Science and Technology A-Applied Sciences and Engineering, **20**(4), pp. 436-445.

[13] Wang M., Li H., Ren J., Gao L., Feng T., Hao Z., Hou D., 2021. Ab initio study on electronic structure and magnetic properties of AlN and BP monolayers with Ti doping. Superlattices and Microstructures, **158**, pp. 107010-107021.

[14] Zhou Y. G., Yang P., Wang Z. G., Zu X. T., Xiao H. Y., Sun X., Gao F., 2011. Electronic and magnetic properties of substituted BN sheets: A density functional theory study. Physical Chemistry Chemical Physics, **13**(16), pp. 7378-7383.

[15] Wang L. C., Zhang Z. C., Ma L. C., Ma L., Zhang, J. M., 2022. First-principles study of hydrogen storage on Li, Na and K-decorated defective boron nitride nanosheets. The European Physical Journal B, **95**(3), pp. 50-64.

[16] Ramirez-de-Arellano J. M., Jiménez G A. F., Magaña L. F., 2021. Catalytic Effect of Ti or Pt in a Hexagonal Boron Nitride Surface for Capturing CO_2. Crystals, **11**(6), pp. 662-675.

[17] Sun P. F., Wang W. L., Zhao X., Dang J. S., 2020. Defective h-BN sheet embedded atomic metals as highly active and selective electrocatalysts for NH_3 fabrication via NO reduction. Physical Chemistry Chemical Physics, **22**(39), pp. 22627-22634.

[18] Liu Y., Yang L. M., Ganz E., 2019. First-principles investigations of single metal atoms (Sc, Ti, V, Cr, Mn, and Ni) embedded in hexagonal boron nitride nanosheets for the catalysis of CO oxidation. Condensed Matter, **4**(3), pp. 65-78.

[19] Deng C., He R., Wen D., Shen W., Li M., 2018. Theoretical study on the origin of activity for the oxygen reduction reaction of metal-doped two-dimensional boron nitride materials. Physical Chemistry Chemical Physics, **20**(15), pp. 10240-10246.

[20] Kalwar B. A., Fangzong W., Soomro A. M., Naich M. R., Saeed M. H., Ahmed I., 2022. Highly sensitive work function type room temperature gas sensor based on Ti doped hBN monolayer for sensing CO_2, CO, H_2S, HF and NO. A DFT study. RSC Advances, **12**(53), pp. 34185-34199.

[21] Zhong S. Y., Wu S. Y., Yu X. Y., Shen G. Q., Yan L., Xu K. L., 2022. First-principles studies of the adsorption and catalytic properties for gas molecules on h-BN monolayer doped with various transition metal atoms. Catalysis Surveys from Asia, **26**(2), pp. 69-79.

[22] Wang M., Meng F., Hou D., Han Y., Ren J., Bai C., Zhou T., 2020. Electronic structure and spin properties study on 2D h-BN nanosheet with Ti or Fe doping. Solid State Communications, **307**, pp. 113803-113809.

[23] Gürel H. H., Salmankurt B., 2017. Binding mechanisms of DNA/RNA nucleobases adsorbed on graphene under charging: first-principles van der Waals study. Materials Research Express, **4**(6), pp. 065401-065409.

[24] Soler J. M., Artacho E., Gale J. D., García A., Junquera J., Ordejón P., Sánchez-Portal D. 2002. The SIESTA method for ab initio order-N materials simulation. Journal of Physics: Condensed Matter, **14**(11), pp. 2745–2779.

[25] Hohenberg P., Kohn W., 1964. Inhomogeneous electron gas. Physical Review, **136**(3B), pp. B864-B872.

[26] Kohn W., Sham L. J., 1965. Self-consistent equations including exchange and correlation effects. Physical Review, **140**(4A), pp. A1133- A1139.

[27] Perdew J. P., Burke K., Ernzerhof M., 1996. Generalized gradient approximation made simple. Physical Review Letters, **77**(18), pp. 3865-3868.

[28] Grimme S., 2006. Semiempirical GGA-type density functional constructed with a long-range dispersion correction. Journal of Computational Chemistry, **27**(15), pp. 1787-1799.

[29] Monkhorst H. J., Pack J. D., 1976. Special points for Brillouin-zone integrations. Physical Review B, **13**(12), pp. 5188-5192.

[30] Gürel H. H., Özçelik V. O., Ciraci S., 2013. Effects of charging and perpendicular electric field on the properties of silicene and germanene. Journal of Physics: Condensed Matter, **25**(30), pp. 305007-305013.

[31] Momma K., Izumi F., 2011. VESTA 3 for three-dimensional visualization of crystal, volumetric and morphology data. Journal of Applied Crystallography, **44**(6), pp. 1272-1276.

[32] Karki R., Khatri K., Adhikari K., Adhikari N. P., Pantha N., 2021. First Principles Study of Structural, Electronic and Magnetic Properties of Defected (Monovacant) Hexagonal Boron Nitride Sheet. Journal of Nepal Physical Society, **7**(4), pp. 19-27.

[33] Anisimov, V. I., Zaanen, J., Andersen, O. K. 1991. Band theory and Mott insulators: Hubbard U instead of Stoner I. Physical Review B, **44**(3), pp. 943-954.

[34] Cococcioni, M., De Gironcoli, S. 2005. Linear response approach to the calculation of the effective interaction parameters in the LDA+U method. Physical Review B, **71**(3), pp. 035105-035121.

[35] Anisimov, V. I., Aryasetiawan, F., Lichtenstein, A. I. 1997. First-principles calculations of the electronic structure and spectra of strongly correlated systems: the LDA+U method. Journal of Physics: Condensed Matter, **9**(4), pp. 767-808.